Mon. Not. R. Astron. Soc. **418,** 2508–2518 (2011) doi:10.1111/j.1365-2966.2011.19641.x

A two-component outer ring and Galactic spiral structure

A. M. Mel'nik[1]★ and P. Rautiainen[2]

[1]*Sternberg Astronomical Institute, 13 Universitetskii pr., Moscow 119992, Russia*
[2]*Astronomy Division, Department of Physics, University of Oulu, PO Box 3000, FI-90014 Oulun yliopisto, Finland*

Accepted 2011 August 16. Received 2011 August 16; in original form 2011 February 28

ABSTRACT

A model of the Galaxy with a ring R_1R_2' can explain some large-scale morphological features of Galactic spiral structure. The Carina–Sagittarius arm could consist of two ascending segments of outer rings R_1 and R_2, which almost touch each other near the Carina region. The Perseus and Crux arms can be partially identified with the descending segments of ring R_2. A model of a two-component outer ring can also explain the existence of some maxima in diagrams of (l, $V_{\rm LSR}$), which are supposed to correspond to directions tangential to the spiral arms. On the basis of numerical simulations, we propose two sketches of the ring structure of the Galaxy that include a bar, two outer rings, an inner ring and nuclear gas condensation, which may be a nuclear ring. Both sketches can explain the position of the Carina–Sagittarius arm with respect to the Sun.

Key words: Galaxy: kinematics and dynamics – Galaxy: structure.

1 INTRODUCTION

The best tracers of Galactic spiral structure are H II regions: gas clouds ionized by young hot stars. Their radio emission penetrates interstellar dust and they can be observed even in distant parts of the Galactic disc. Heliocentric distances r for faraway H II regions ($r > 6$ kpc) are usually determined from kinematic models under the assumption that velocity deviations from the rotation curve are zero. The kinematic method yields an unambiguous distance for objects located outside the solar circle ($R > R_0$), but gives two possible distances corresponding to the same line-of-sight velocity inside the solar circle ($R < R_0$, where R is the Galactocentric distance). The choice between 'near' and 'far' distances requires additional information, usually data on the absorption/emission lines of H I/H_2CO or self-absorption in the H I line. The method is based on the analysis of velocities of foreground clouds (Anderson & Bania 2009).

Georgelin & Georgelin (1976), using the distribution of 100 H II regions with an excitation parameter of more than $U > 70\,{\rm pc\,cm^{-2}}$, have proposed a four-armed spiral pattern with a mean pitch angle of the spiral arms of $i \approx 12^\circ$. Their model can also explain the existence of so-called tangential directions – lines of sight corresponding to maxima in the thermal radio continuum, H I and CO emission – which are associated with the tangents to the spiral arms. These directions were first determined from the analysis of longitude–velocity diagrams in H I (Burton & Shane 1970; Kerr 1970; Simonson 1970), which exhibited the distribution of gas temperature in coordinates (l, $V_{\rm LSR}$), where l is the Galactic longitude and $V_{\rm LSR}$ the heliocentric line-of-sight velocity V_r corrected for solar motion toward the apex, averaged over some range of Galactic latitude b. The original model by Georgelin & Georgelin (1976) has been developed on the basis of new data (Lockman 1979; Downes et al. 1980; Caswell & Haynes 1987; Russeil 2003; Watson et al. 2003; Paladini, Davies & DeZotti 2004; Russeil, Adami & Georgelin 2007; Hou, Han & Shi 2009; Efremov 2011).

Russeil (2003) has grouped H II regions and molecular clouds into complexes of star formation, which enables her to decrease the random errors in determination of mean velocities and kinematic distances. Locations of the spiral arms supposed by Russeil (2003) practically coincide with those obtained by Georgelin & Georgelin (1976), although the spiral structure generally becomes more symmetrical. Russeil (2003) supposes that her sample of complexes including H II regions with high excitation parameter ($U > 60\,{\rm pc\,cm^{-2}}$) is complete over all the Galactic disc. For determination of kinematic distances she has used a nearly flat rotation curve derived from objects with known photometric distances.

There are also other indicators of Galactic spiral structure. One of them is giant clouds of molecular hydrogen (GMCs), with size $\sim$40 pc and mass 10^4–$10^6\,{\rm M_\odot}$. Cohen, Dame & Thaddeus (1986) showed that GMCs outlined the Carina arm well. Dame et al. (1986) solved the ambiguity in the choice between the two kinematic distances in the first quadrant and selected objects in the Sagittarius arm. Grabelsky et al. (1988) compiled a catalogue of GMCs in the region $270 < l < 300^\circ$ and identified objects in the Carina arm. Also, neutral hydrogen is concentrated in the spiral arms (Oort, Kerr & Westerhout 1958; Kerr 1962) and is distributed quite non-uniformly outside the solar circle (Henderson, Jackson & Kerr 1982; Kalberla et al. 2005; Levine, Blitz & Heiles 2006).

We will show that a two-component outer ring of class R_1R_2 can also explain many large-scale morphological features of Galactic

★E-mail: anna@sai.msu.ru

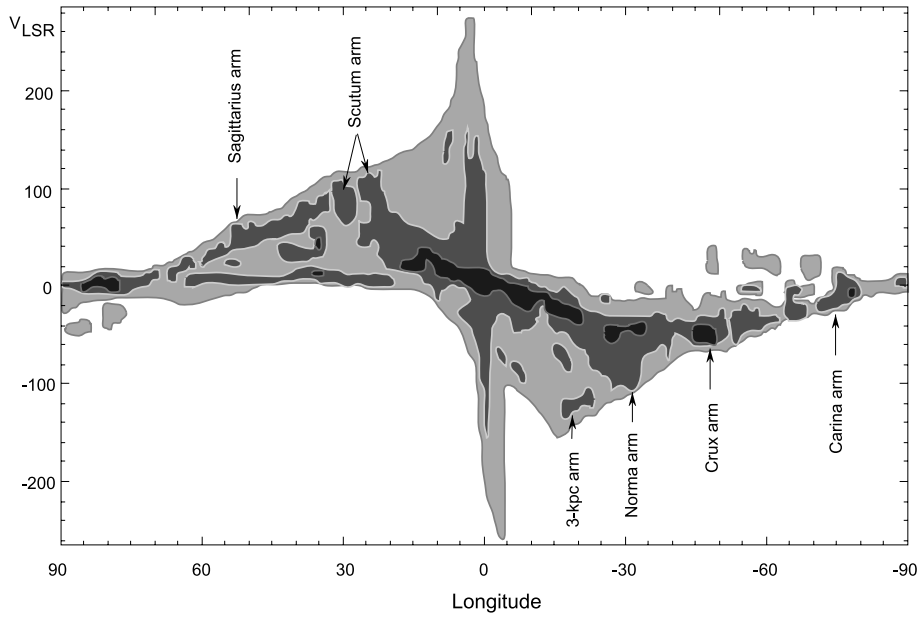

Figure 1. Sketch of the diagram (l,$V_{\rm LSR}$) of the ^{12}CO distribution (Dame et al. 2001). The emission is averaged in the range $b = \pm 2^\circ$. It also indicates the positions of maxima corresponding to the directions tangential to the spiral arms.

spiral structure. This paper has the following structure. Section 2 is devoted to tangential directions, the dynamical and kinematic aspects of the problem are discussed in Section 3, a brief description of dynamical models including outer rings is given in Section 4 and Section 5 presents the results of a comparison of our models with observations.

2 TANGENTIAL DIRECTIONS AND THE NAMES OF THE SPIRAL ARMS

Englmaier & Gerhard (1999) and Vallée (2008) compiled information about directions tangential to the spiral arms. Generally, the tangential directions are connected with the existence of some intensity maxima in diagrams of (l, $V_{\rm LSR}$). Fig. 1 shows the distribution of ^{12}CO composed by Dame, Hartmann & Thaddeus (2001). Velocities of more than $\pm 150\,{\rm km\,s^{-1}}$ in the central region ($|l| \leq 10^\circ$) can be explained by the presence of elliptical orbits in the central region. In general, however, gas at positive longitudes, $10 < l < 90^\circ$, has positive velocities $V_{\rm LSR}$ and gas at negative longitudes, $-90 < l < -10^\circ$, negative velocities. The extreme velocities in each direction are often called terminal velocities. Besides this, the diagrams demonstrate the ridge-like intensity maxima that are often associated with the spiral arms. The directions at which the 'ridges' reach the curves of terminal velocity are thought of as tangential directions (Table 1).

Table 1. Directions tangential to the spiral arms.

N	longitude	Name	Other name
1	$l \sim 284^\circ$	Carina arm	
2	$l \sim 310^\circ$	Crux arm	Centaurus arm
3	$l \sim 327^\circ$	Norma arm	Norma–3-kpc arm
4	$l \sim 339^\circ$	3-kpc arm	start of Perseus arm
5	$l \sim 25, 31^\circ$	Scutum arm	
6	$l \sim 51^\circ$	Sagittarius arm	

Note also the presence of bright emission at $l = 80^\circ$ corresponding to the Cygnus region (l = 73–78°, r = 1.5 kpc), which is usually directly associated with the Local arm or spur (its other name is the Orion–Cygnus arm) and is therefore excluded from consideration.

The connection of bright spots in the diagrams of (l, $V_{\rm LSR}$) with a certain distance should be taken with great caution: in reality they can consist of a chain of clouds extended for several kpc along the line of sight (Adler & Roberts 1992). The problem is that different models of gas motion in the Galaxy can produce very similar diagrams of (l, $V_{\rm LSR}$).

Fig. 2 illustrates the idea of tangential directions. It shows a regular spiral pattern with parameters $i = 12.^\circ 8$, $r_0 = 2.1$ kpc, $\theta_0 = -20^\circ$ and $m = 4$ taken from the paper by Vallée (2008), as well as the tangential directions. It also exhibits a distribution of giant star-forming complexes from the catalogue by Russeil (2003). We can clearly see that every ray is tangent (or passes very close to the tangent) to the spiral arm. On the other hand, only the Carina arm is outlined well by star-forming complexes.

Note that the naming of the arms in the literature is somewhat confusing: the Norma arm is sometimes called the Norma–3-kpc arm, but the 3-kpc arm, in turn, is also termed 'the start of the Perseus arm' (see also Table 1). Another example is the Cygnus arm, which can easily be confused with the Cygnus region situated near the Sun ($r = 1.5$ kpc). This outer arm is also sometimes called the 'Perseus + I arm' or 'Norma–Cygnus arm' (Vallée 2005, 2008).

There are no tangential directions to the outer Cygnus arm ($70 < l < 220^\circ$, r = 5–9 kpc, R = 11–15 kpc), because it lies outside the solar circle. Interestingly, the Cygnus arm is absent on the schema supposed by Georgelin & Georgelin (1976). Its appearance is due to two things: the principle of symmetry and the discovery of new H II regions. Efremov (1998, 2011) identifies the H I superclouds outlining the Carina–Sagittarius arm and shows that the arm symmetrical to it does not coincide with the Perseus arm but lies beyond it. Additionally, Russeil (Russeil 2003; Russeil et al. 2007) discoveres many star-forming complexes in the region $70 < l < 220^\circ$ in the distance range r = 4–10 kpc which cannot belong to the Perseus arm.

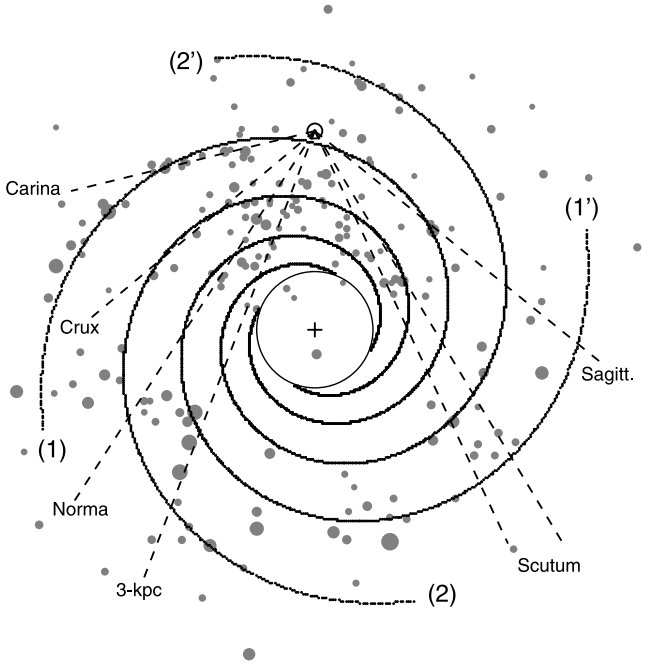

Figure 2. Regular spiral pattern with parameters of logarithmic spirals: $i = 12.^{\circ}8$, $r_0 = 2.1$ kpc, $\theta_0 = -20^{\circ}$ and $m = 4$ (Vallée 2008). 1: Sagittarius–Carina arm; 2: Scutum–Crux arm; 1′: Norma–Cygnus arm; 2′: Perseus arm. The figure also shows the tangential directions to the spiral arms. Giant star-forming complexes ($U > 60\,\mathrm{pc\,cm^{-2}}$) from the catalogue by Russeil et al. (2007) are depicted by grey circles with size proportional to the excitation parameter.

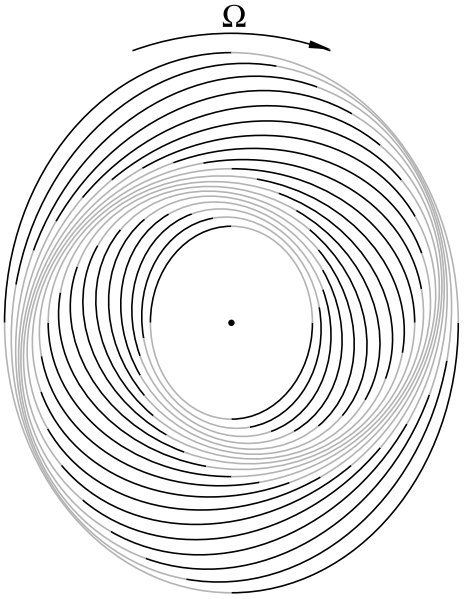

Figure 3. Segments of stellar orbits with negative and positive radial velocity V_R in the trailing density-wave spiral arms located inside the CR. The galaxy rotates clockwise. Motions are considered in a reference frame corotating with the spiral pattern, in which stars also rotate clockwise. The ascending segments of ellipses ($V_R > 0$) are shown in black whereas the descending ones ($V_R < 0$) are shown in grey. Inside the CR, crowding of orbits occurs on the descending segments of ellipses.

3 DYNAMICAL AND KINEMATICAL ASPECTS OF THE PROBLEM

The models suggested by Georgelin & Georgelin (1976) and developed in subsequent papers leave open many questions. At the moment no N-body simulations with realistic rotation curve and size of the bar can reproduce the classical four-armed pattern. The main problem concerns lack of a dynamical mechanism that could support a four-armed spiral pattern occupying a large part of the galactic disc (see surveys by Toomre 1977; Athanassoula 1984; Binney & Tremaine 2008).

The concept of density-wave theory (Lin & Shu 1964; Bertin & Lin 1996), where spiral arms form at places of crowding of the orbits, deserves special attention. A lot of researchers think that at least two major spiral arms in the Galaxy are density-wave spiral arms. However, density waves create a specific distribution of velocities in the young disc population that is forming due to adjustment of the epicyclic motions of stars in accordance with orbital rotation (Lin, Yuan & Shu 1969). Kalnajs (1973) suggests that one considers stellar orbits in a reference frame corotating with the speed of the spiral pattern Ω_p, in which the orbits look like pure ellipses or ellipses with 'dimples'. If we know the direction of rotation of disc stars in the adopted frame, then we can divide their orbital ellipses into ascending and descending segments, where stars move away ($V_R > 0$) and toward ($V_R < 0$) the Galactic Centre, respectively. Fig. 3 illustrates the idea that orbit-crowding occurs at the descending or ascending segments of ellipses, and the choice between them depends on the sense of orbital rotation. This must be viewed in a reference frame rotating with speed Ω_p in which the sense of rotation is determined by the position of the corotation radius (CR) with respect to the region considered. Thus, knowledge of the direction of the radial component V_R of velocity in the spiral arms allows us to restrict the region in which the CR can be located and thereby roughly estimate the value of the angular speed of the spiral pattern Ω_p.

The study of the kinematics of young stars in regions of intense star formation yields an unexpected distribution of velocities. The radial component V_R of the velocity in the Carina, Cygnus and Perseus regions is directed toward the Galactic Centre ($V_R < 0$), while it is directed away from it ($V_R > 0$) in the Sagittarius region and in the Local System (Mel'nik, Dambis & Rastorguev 1999, 2001; Mel'nik 2003; Sitnik 2003; Mel'nik & Dambis 2009). This means that the Perseus and Sagittarius regions cannot be parts of the same density-wave spiral pattern rotating with one pattern speed. Note that a two-armed model of the Galactic spiral structure with an angular speed $\Omega_\mathrm{p} = 13.5\,\mathrm{km\,s^{-1}\,kpc^{-1}}$ (Lin et al. 1969) can reproduce well the kinematics in the Perseus region (Roberts 1972; Burton & Bania 1974; Humphreys 1976, and other papers). However, the kinematics of the Sagittarius region indicate that it must be located outside the CR which corresponds to a speed of more than $\Omega_\mathrm{p} > 38\,\mathrm{km\,s^{-1}\,kpc^{-1}}$ (Mel'nik 2006).

There is much evidence that our Galaxy includes a bar. Estimates of the length of the bar have increased from an initial $R_\mathrm{bar} = 2$–3 kpc (Binney et al. 1991; Blitz & Spergel 1991; Blitz et al. 1993) to the current values $R_\mathrm{bar} = 3$–5 kpc (Benjamin et al. 2005; Babusiaux & Gilmore 2005; Habing et al. 2006; Cabrera-Lavers et al. 2007; Pohl, Englmaier & Bissantz 2008; Gerhard 2011). Dynamical models of a gaseous medium moving in the Galactic potential perturbed by the bar reproduce the so-called 'parallelograms' on the diagrams of (l, V_LSR) in the central region (Englmaier & Gerhard 1999; Fux 1999; Weiner & Sellwood 1999; Englmaier & Gerhard 2006). The general consensus is that the major axis of the bar is oriented in the direction $\theta_\mathrm{b} = 15$–45° in such a way that the end of the bar closest to the Sun lies in the first quadrant.

The concept that the Galaxy can include several modes rotating with different angular speeds was actively developed in the early 2000s. The rapidly rotating bar ($\Omega_b = 40$–$60\,\mathrm{km\,s^{-1}\,kpc^{-1}}$) and the slower mode ($\Omega_{sp} = 20$–$40\,\mathrm{km\,s^{-1}\,kpc^{-1}}$) could explain the gas kinematics in the central region and at larger distances, respectively (Bissantz & Gerhard 2002; Bissantz, Englmaier & Gerhard 2003). However, application of a two-mode model to the Galaxy appears to be much harder than expected. On the one hand there are many dynamical models, in which the disc forms a pattern rotating more slowly than the bar (Sellwood & Sparke 1988; Masset & Tagger 1997; Rautiainen & Salo 1999, 2000). On the other hand, after introducing physical units the strongest slow mode turns out to have a pattern speed of $\Omega_{sp} \approx 30\,\mathrm{km\,s^{-1}\,kpc^{-1}}$, which is too high to explain the kinematics of young stars in the Perseus region.

In parallel with the concept of modes, a different approach has been developed. Here the spiral arms are regarded as a subsequent generation of short-lived spiral perturbations connected with each other through resonances: the CR of each next wave is located at one of the resonances of the previous wave (Sellwood & Lin 1989; Sellwood & Kahn 1991; Sellwood 2000, 2011). Nevertheless, it is questionable whether this approach can explain the existence of long spiral arms similar to the Carina one in the Galaxy (Fig. 2).

4 MODELS OF THE GALAXY INCLUDING THE OUTER RING

The essential characteristic of galaxies with outer rings and pseudo-rings – incomplete rings made up of spiral arms – is the presence of a bar (Buta 1995; Buta & Combes 1996). Since the outer rings have an elliptic form, the broken outer rings (pseudo-rings) resemble two tightly wound spiral arms. Two main classes of outer rings and pseudo-rings have been identified: R_1 rings (R'_1 pseudo-rings) elongated perpendicular to the bar and R_2 rings (R'_2 pseudo-rings) elongated parallel to the bar. In addition, there is a combined morphological type $R_1R'_2$ which shows elements of both classes. The R_2 rings have an elliptical shape, but the R_1 rings are often 'dimpled' near the bar ends (Buta 1995; Buta & Crocker 1991).

The test-particle simulations (Schwarz 1981; Byrd et al. 1994; Rautiainen & Salo 1999) and N-body simulations (Rautiainen & Salo 2000) show that the outer rings are typically located in the region of the outer Lindblad resonance (OLR). Schwarz (1981) connected two main types of outer rings with two main families of periodic orbits existing near the OLR of the bar (Contopoulos & Papayannopoulos 1980; Contopoulos & Grosbol 1989). The stability of orbits enables gas clouds to follow them for a long time period. The R_1 rings are supported by $x_1(2)$ orbits (using the nomenclature of Contopoulos & Grosbol 1989) lying inside the OLR and elongated perpendicular to the bar, while the R_2 rings are supported by $x_1(1)$ orbits situated a little outside the OLR and elongated along the bar.

The bar semi-major axis in the Galaxy is supposed to lie in the range $a = 3$–$5\,\mathrm{kpc}$. For a flat rotation curve and a fast-rotating bar this means that the bar angular speed Ω_b is limited to the interval $\Omega_b = 40$–$70\,\mathrm{km\,s^{-1}\,kpc^{-1}}$ and the OLR of the bar is located in the solar vicinity: $|R_{OLR} - R_0| < 1.5\,\mathrm{kpc}$. Studies of the kinematics of old disc stars in the immediate solar vicinity, $r < 250\,\mathrm{pc}$, revealed a bimodality in the distribution of (u, v) velocities that was also interpreted as a result of the solar location near the OLR of the bar (Kalnajs 1991; Dehnen 2000; Fux 2001; Chakrabarty 2007; Minchev et al. 2010, and other papers). Thus, the presence of an outer ring in the Galaxy is a plausible possibility to consider.

In addition to the outer rings, the Galaxy can include an inner ring or pseudo-ring surrounding the bar, which manifests itself in the so-called 3-kpc arm(s) (Fux 1999; Dame & Thaddeus 2008; Churchwell et al. 2009). Also, a hypothesis regarding the presence of a nuclear ring with a major axis of $\sim$1 kpc is considered (Rodriguez-Fernandez & Combes 2008).

Using the simulation code developed by H. Salo (Salo 1991; Salo & Laurikainen 2000) we have constructed two different types of models (models with analytical bars and N-body simulations) that reproduce the kinematics of OB associations in the Perseus and Sagittarius regions. The kinematics of young stars in the Perseus region indicate the existence of an R_2 ring, while velocities in the Sagittarius region suggest the presence of an R_1 ring in the Galaxy. Our models have nearly flat rotation curves. The major and minor axes of the bar have values of $a = 4.0$ and $b = 1.2\,\mathrm{kpc}$. The value of the solar position angle with respect to the bar θ_b providing the best agreement between the model and observed velocities is $\theta_b = 45 \pm 5^\circ$. The bar angular speed lies in the range $\Omega_b = 42$–$55\,\mathrm{km\,s^{-1}\,kpc^{-1}}$ (Mel'nik & Rautiainen 2009; Rautiainen & Mel'nik 2010, hereafter Papers I and II, respectively).

In the present paper we use the distribution of OB particles in 'model No. 3' obtained in the series of models with analytical bars for the time $T = 15$ ($\sim$1 Gyr). Model 3 was chosen due to the presence of the inner ring, which still persists by $T = 1$ Gyr. As for the outer rings, all models considered produce a similar distribution of OB particles on the galactic periphery (Paper I). We also use the distribution of gas and stellar particles in the N-body model averaged for the time interval $T = 5$–6 Gyr. Averaging over a large time interval reduces the influence of slow modes and occasional perturbations (Paper II).

5 RESULTS

5.1 Ring $R_1R'_2$ and the distribution of giant star-forming complexes

In this section we will use data from the catalogue by Russeil et al. (2007), particularly the sample of giant star-forming complexes with an excitation parameter of more than $U > 60\,\mathrm{pc\,cm^{-2}}$, which includes 194 regions in the range of Galactocentric distances $0 < R < 12\,\mathrm{kpc}$, 76 per cent of them having only kinematic distances.

The distance scale in our models (Papers I and II) is adjusted to the so-called short distance scale of classical Cepheids (Berdnikov, Dambis & Vozyakova 2000). The distance scale for star-forming complexes from the catalogue by Russeil et al. (2007), r_0, is close to that for OB associations (Humphreys & McElroy 1984; Blaha & Humphreys 1989), so to match it with the short distance scale we used the same scaling factor of $f = 0.8$ ($r = fr_0$) that was used for reducing the distance scale for OB associations (Sitnik & Mel'nik 1996; Dambis, Mel'nik & Rastorguev 2001; Mel'nik & Dambis 2009).

Fig. 4 exhibits the distribution of giant star-forming complexes and that of OB particles from the series of models with analytical bars (Paper I). It also demonstrates the position of the regions of intense star formation studied in Papers I and II. The Sagittarius region ($x = 0.5$, $y = 6.0\,\mathrm{kpc}$) lies on a segment of the ring R_1, whereas the Carina region ($x = -1.5$, $y = 6.5\,\mathrm{kpc}$) occupies the intermediate position between the two outer rings in the place where they come closest to each other. The Perseus region ($x = 2.0$, $y = 8.0\,\mathrm{kpc}$) and the Local System ($x = 0.0$, $y = 7.4\,\mathrm{kpc}$) belong to the ring R_2, while the Cygnus region ($x = 1.5$, $y = 6.9\,\mathrm{kpc}$) appears to

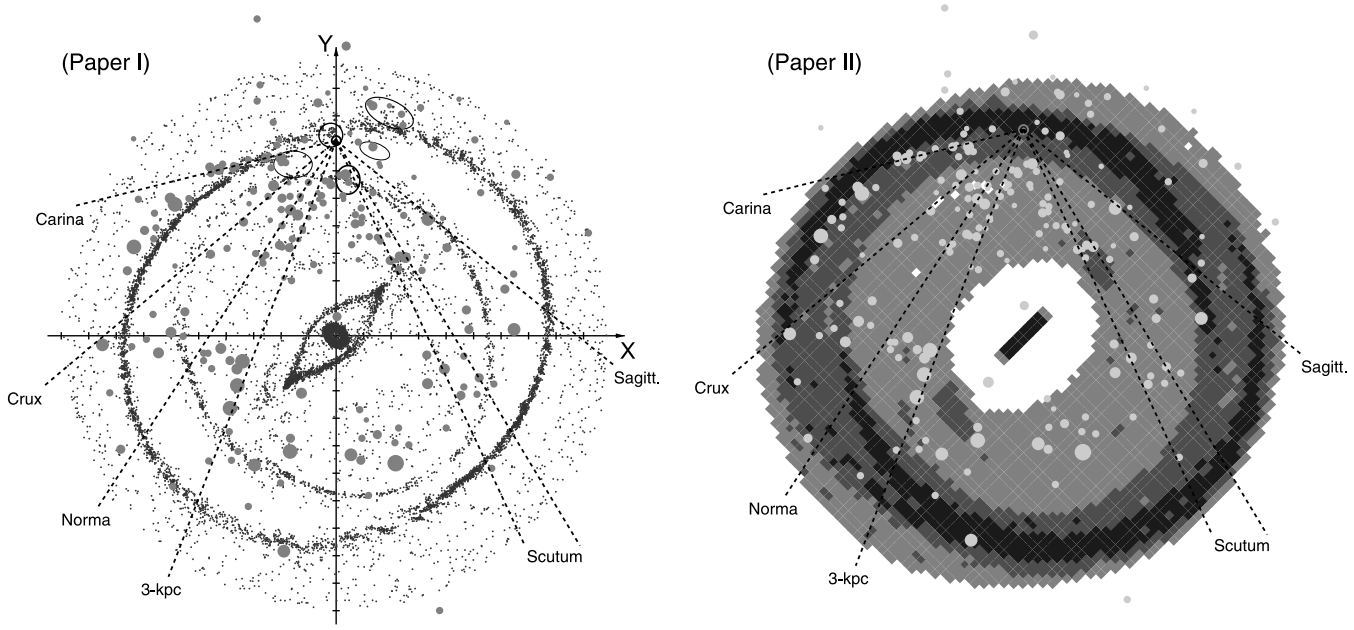

Figure 4. Comparison of the distribution of model particles with the distribution of giant star-forming complexes (Russeil et al. 2007). Left: distribution of OB particles (black points) in a model with an analytical bar (Paper I). The boundaries of the regions of intense star formation studied in Papers I and II are also indicated. A division on the X and Y axis corresponds to 1 kpc. Right panel: gas-density distribution in the N-body model averaged in small squares (Paper II). The light grey, dark grey and black colours represent squares containing an increasing number of particles. Giant complexes ($U > 60\,\mathrm{pc\,cm^{-2}}$) are depicted as circles with size proportional to the excitation parameter U. The tangential directions to the spiral arms are also shown (Table 1). The adopted value for the solar position angle with respect to the bar is $\theta_\mathrm{b} = 45^\circ$. The Galaxy rotates clockwise.

lie in the inter-ring space. The Galactocentric distance of the Sun is adopted to be $R_0 = 7.1$ (Rastorguev et al. 1994; Dambis, Mel'nik & Rastorguev 1995; Glushkova et al. 1998).

The outer rings can be divided into ascending ($V_R > 0$) and descending ($V_R < 0$) segments. On the ascending segments (segments C–D–E and 5–6–7 in fig. 6 of Paper I), the Galactocentric distance R decreases with increase of the azimuthal angle θ. This becomes clear if we remember that closed orbits emerge only in the reference frame corotating with the bar. The outer rings lie near the OLR of the bar where disc objects rotate more slowly than the bar; therefore in the reference frame corotating with it they will move in a direction opposite to that of Galactic rotation, i.e. counterclockwise. On the descending segments of the outer rings (segments 3–4–5 and E–F–G in fig. 6 of Paper I) the Galactocentric distance R increases with increasing θ. Note also that the ascending segments of the outer rings can be regarded as fragments of the trailing spiral arms and the descending ones as fragments of the leading spiral arms.

The Carina arm is often regarded as the major spiral arm in the Galaxy. It begins near the Carina region and unwinds counterclockwise along the Galactocentric angle at $|\Delta\theta| \approx 90^\circ$. It is evident that the star-forming complexes related to the Carina arm fall nicely on the ascending segment of ring R_2: the deviation does not exceed 15 per cent of the heliocentric distance r. Note also that the objects related to the Sagittarius arm are situated near the ascending segment of ring R_1. Although most researchers consider the Carina–Sagittarius arm as a single spiral arm, it could consist of two ascending segments of outer rings R_1 and R_2 that almost touch each other near the Carina region ($x = -1.5$, $y = 6.5$ kpc). It is difficult to say anything about another pair of ascending segments of the outer rings, but it is possible that they could be identified with the Norma–Cygnus arm symmetrical to the Carina–Sagittarius one. If the ascending segments of the outer rings were much brighter than the descending ones, then the Galactic spiral structure would be considered as two-armed. In this context, the four-armed pattern suggests significant brightness of the descending segments. The Perseus and Crux arms can be partially identified with the descending segments of ring R_2. Interestingly, the giant complex 475 ($l = 352.^\circ8$, $b = 1.^\circ3$) (Russeil et al. 2007), which is the brightest in the Crux arm and practically determines its position, falls exactly on the descending segment of ring R_2 (see its location in Fig. 8a, later).

We also studied the position of the outer rings with respect to the tangential directions. It turned out that a model of a two-component outer ring can also explain the appearance of some of these directions: the line of sight in the direction $l = 284^\circ$ is almost tangential to the outer ring R_2, and the rays in the directions $l = 310^\circ$ and 51° are tangents to the ring R_1 (Fig. 4). In addition, the lines of sight in the range $l = 25$–31° point to the end of the bar closest to the Sun. However, the directions $l = 327^\circ$ and 339° cannot be identified with any tangents to the rings or to the bar.

Fig. 4 also exhibits the gas-density distribution in the N-body model (Paper II). As was expected, the lines of sight in the directions $l = 284^\circ$ (Carina arm) and 51° (Sagittarius arm) cross a huge gas column on their way through the combined R_1R_2 outer ring. The rays in the direction $l = 25$–31° intersect a region of high gas content located near the end of the bar. In distinction from models with analytical bars, the N-body model retains a lot of gas near the bar ends.

5.2 Ring R_1R_2' and diagrams (l, V_LSR)

We assume that the variations in the ^{12}CO antenna temperature are caused by variations in the number of small unresolved molecular cloudlets falling within the field of the telescope (Mihalas & Binney 1981). If we associate these small clouds with gas particles in our models, then the most bright regions in the observational maps must correspond to regions of high column density in the model diagrams.

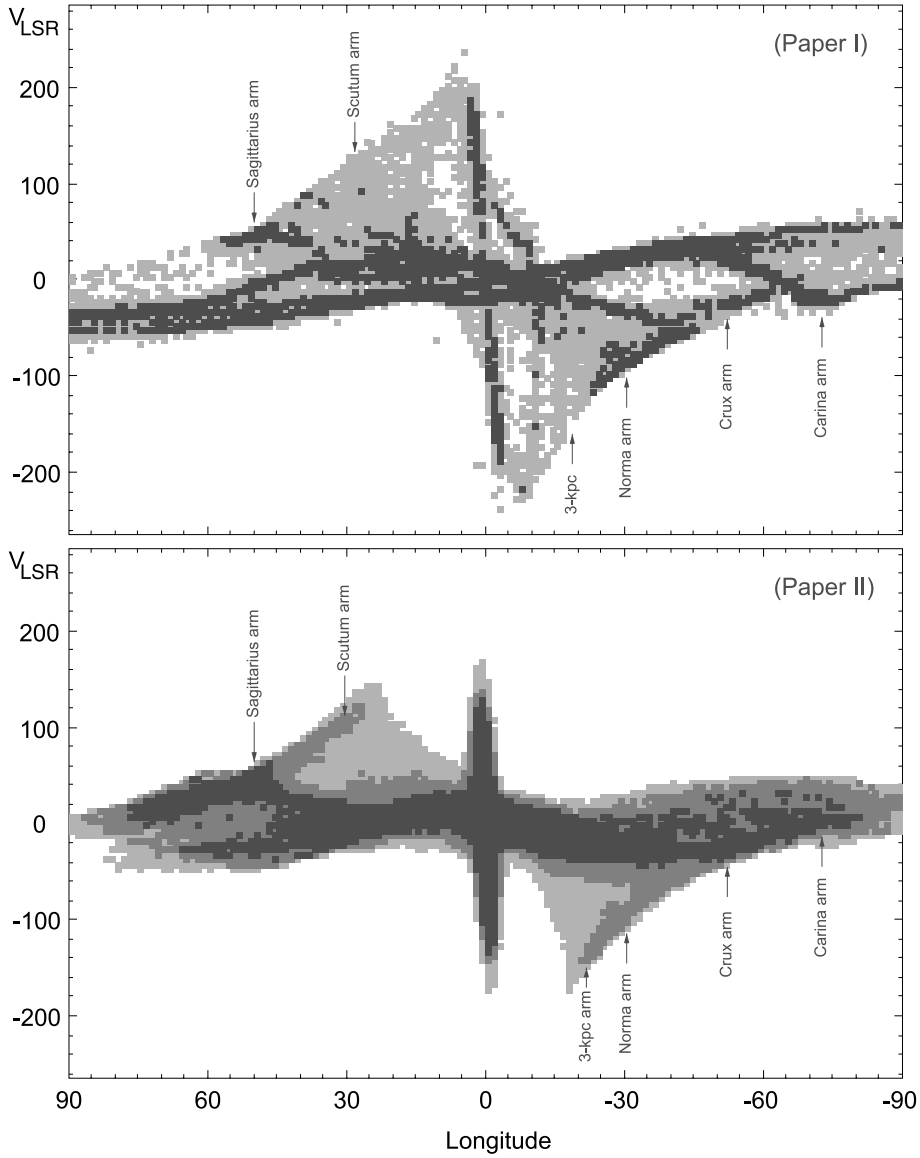

Figure 5. Diagrams of (l, $V_{\rm LSR}$) built for a model with an analytical bar (Paper I) and for an N-body simulation (Paper II). The darker colours correspond to cells with an increasing number of particles n. In the upper panel, two grey shades represent cells with n below and above the average value $\overline{n}$ ($\overline{n} = 11$). In the lower panel three grey shades show cells with $10 < n < \overline{n}$, $\overline{n} < n < 2\overline{n}$ and $n > 2\overline{n}$ ($\overline{n} = 427$). The maxima connected with the directions tangential to the spiral arms are also indicated.

Fig. 5 shows the distribution of gas particles in the plane (l, $V_{\rm LSR}$) built for model with an analytical bar (Paper I) and for the N-body simulation (Paper II). It also indicates the positions of the observational maxima near the terminal velocity curves, which are supposed to correspond to the directions tangential to the spiral arms. It is seen that the model diagrams reproduce the intensity maxima in the direction of the Carina, Crux, Norma and Sagittarius arms. Moreover, the N-body model also creates maxima in the directions of the Scutum and 3-kpc arms. Our models also produce a velocity peak of more than $|V_{\rm LSR}| > 150\,{\rm km\,s^{-1}}$ in the central region, $-5 < l < 5^\circ$.

Fig. 6 demonstrates the distribution of model particles in the Galactic plane (Paper I) and their positions in the diagram of (l, $V_{\rm LSR}$). The Galactic plane is divided into annuli. The fan-shaped structure of the diagram is obvious: particles located at different annuli occupy different strip-like zones in the diagram. The larger the radius of the annulus, the larger the angle between the corresponding strip and the vertical axis. Interestingly, the central peak is formed not only by objects of the nuclear ring but also by particles of the inner ring.

Note that our model diagrams of (l, $V_{\rm LSR}$) do not reproduce the so-called 'Molecular Ring' in the observed CO survey (Fig. 1), the ridge of enhanced emission that extends from the Scutum tangential point to the Norma one (Dame et al. 2001). This observational feature is sometimes interpreted as a molecular ring (Binney et al. 1991) or as spiral arms emanating from the bar (Fux 1999). In any case, our models need some modification to keep more gas near the bar ends.

5.3 Ring model of the Galaxy

Let us consider a new model of the Galaxy that includes two outer rings, the inner ring and the nuclear ring. Fig. 7 represents a basic diagram of galactic ring structure, composed on the basis of

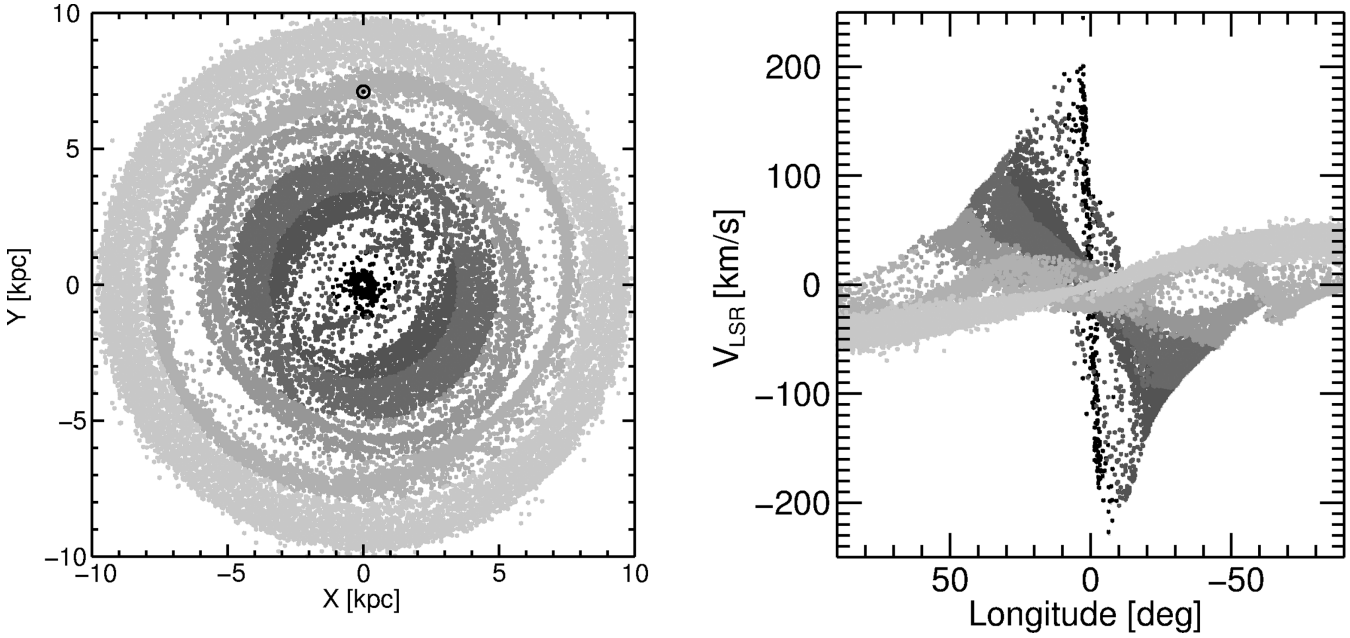

Figure 6. Left: the distribution of gas particles in the Galactic plane in a model with an analytical bar (Paper I). The size of the frame is 20 kpc. Particles located in different annuli are shown in different grey shades. Right: the position of particles selected in the diagram of (l, V_{LSR}). The diagram has a fan-shaped structure: objects of different annuli are located in strip-like zones turned at different angles to the vertical axis. The larger the annulus, the greater the angle between the corresponding strip and the vertical axis.

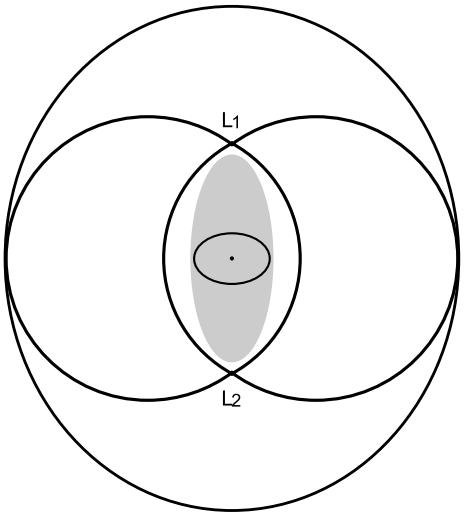

Figure 7. Basic model of galactic ring structure. It includes a bar (grey ellipse), a nuclear ring which is represented by an ellipse aligned perpendicular to the bar, an inner ring elongated along the bar, an '8'-shaped outer ring R_1 stretched perpendicular to the bar and an outer ring R_2 aligned with the bar.

sketches designed by Buta (1986). The resonance rings are supported by periodic orbits, which are elongated parallel or perpendicular to the bar and change their orientation near the OLR, CR and ILR(s); some chaotic orbits also share similar characteristics (Contopoulos & Papayannopoulos 1980; Contopoulos & Grosbol 1989). However, not only resonant processes determine the formation of ring-like structures in galactic discs. They are also affected by gas flow outwards or inwards due to torque from the bar. The central region often includes inner spiral arms that connect Lagrangian points L_1 and L_2 with the nuclear ring or with the galactic centre; these are shocks caused by the bar (Athanassoula 1992). Note also that outer rings R_1 and R_2 in the basic sketch connect with each other, but such a connection is sometimes absent in numerical simulations and in images of real galaxies (for example NGC 1211). The connection between the inner ring and the outer ring R_1 can also be missing (for example NGC 3081: Buta, Corwin & Odewahn 2007).

Application of the basic ring structure to the Galaxy does not give an unambiguous picture. On the basis of numerical simulations, we designed two sketches of the Galactic spiral structure (Fig. 8). In sketch A we try to reproduce the distribution of gas particles in the model with an analytical bar (Paper I) and in sketch B the distribution of gas and star particles in the N-body simulation (Paper II). Both sketches have many similar features: the bar is represented as a grey ellipse with semi-axes $a = 4.0$ and $b = 1.2$ kpc, the position angle of the Sun with respect to the bar equals $\theta_b = 45^\circ$ and the outer ring R_2 is approximated by an ellipse elongated along the bar with semi-axes $a_2 = 8.0$ and $b_2 = 7.2$ kpc, which is in good agreement with the distribution of OB particles in models with analytical bars (Paper I). The main differences in sketches A and B lie in the size of ring R_1, the shape of the inner ring and the orientation of the central gas condensation.

In sketch A, the CR of the bar lies at $R = 4.0$ kpc, just at the bar ends. The R_1 ring only reaches a radius of $R = 6.0$ kpc, thereby forming a gap between the two outer rings. The inner structure is represented by the pointed inner ring connecting the bar ends with the nuclear ring. The connection between the inner ring and outer ring R_1 is also absent. The nuclear ring is represented by an ellipse elongated perpendicular to the bar with semi-axes $a_n = 0.8$ and $b_n = 0.6$ kpc.

In sketch B, the CR of the bar is located at $R = 4.6$ kpc. The R_1 ring begins near the CR and reaches for the OLR of the bar so that there is no gap between the rings R_1 and R_2. In the N-body simulation, the ring R_1 forms mainly in the stellar population. The gaseous inner

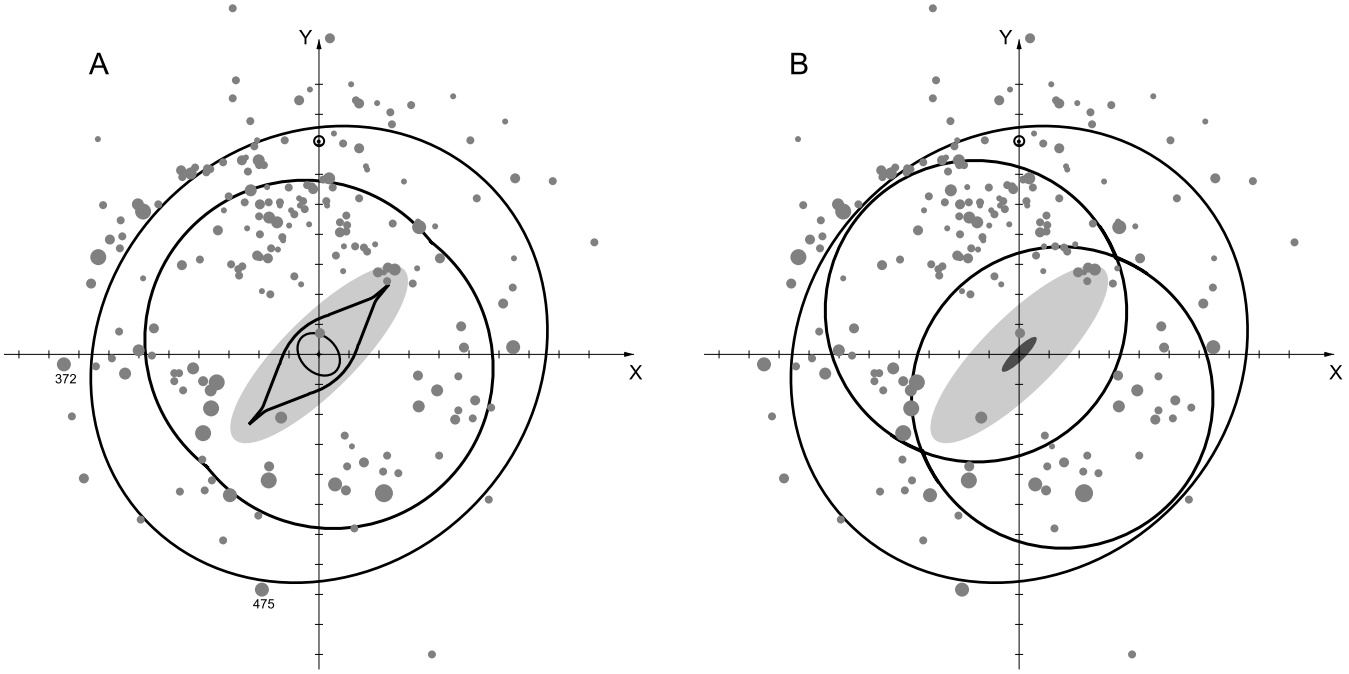

Figure 8. Ring structure applied to the Galaxy. In both sketches the bar is represented as a grey ellipse with semi-axes $a = 4.0$ and $b = 1.2$ kpc. The position angle of the Sun with respect to the bar is $\theta_b = 45^\circ$. The outer ring R_2 is shown by an ellipse elongated along the bar with semi-axes $a_2 = 8.0$ and $b_2 = 7.2$ kpc. Sketch A is determined by the distribution of particles in the model with an analytical bar (Paper I) while sketch B is based on the distribution of particles in N-body simulations (Paper II). We can see a gap between the two outer rings R_1 and R_2 in sketch A but it is absent in sketch B. Sketch A has the more elongated and smaller inner ring in comparison with that in sketch B. There are also some differences in the shape and orientation of nuclear gas condensation in sketches A and B. Also shown is the distribution of giant star-forming complexes ($U > 60\,\mathrm{pc\,cm^{-2}}$, Russeil et al. 2007). The value of R_0 adopted is $R_0 = 7.1$ kpc.

ring has a rounder shape here compared with sketch A. The central gas condensation is represented by an ellipse elongated along the bar with semi-axes $a_n = 0.8$ and $b_n = 0.2$ kpc.

Both sketches can easily explain the location of the Sagittarius–Carina arm with respect to the Sun. This arm can consist of two ascending segments of outer rings R_1 and R_2. At the first glance, objects of the Carina arm form a more open structure, but this impression is mainly based on the position of the complex 372 ($l = 311.^\circ2$, $b = -0.^\circ4$) (Russeil et al. 2007, see Fig. 8a). However, we can move it along the line of sight so that it falls exactly on ring R_2 (for more details see Section 5.4).

Mid-infrared observations show an excess of old stars in the direction of the Centaurus ($l \approx -50^\circ$) and Scutum ($l \approx 25$–31°) arms but not in the direction of the Sagittarius arm ($l \approx +50^\circ$) (Drimmel 2000; Churchwell et al. 2009). Sketch A can easily explain an increase in the density of old stars in the direction of the Centaurus arm (another name for the Crux arm). The line of sight in the direction $l \approx -50^\circ$ is nearly tangent to the outer ring R_1 (Fig. 4). Observations and modelling show that R_1 rings can be formed in the stellar subsystem, but R_2 rings usually appear only in the gas component (Byrd et al. 1994; Rautiainen & Salo 2000). However, we cannot explain the absence of an excess of old stars in the direction of the Sagittarius arm: in our model, the Centaurus ($l \approx -50^\circ$) and Sagittarius ($l \approx +50^\circ$) arms are segments of the same ring R_1 and consequently must have the same nature.

The distribution of optical objects in the Galactic plane also provides some evidence for the existence of a gap between the Sagittarius and Carina regions. Humphreys (1979) shows that OB associations and young open clusters are concentrated in either the Sagittarius or the Carina region, but not in between. Recent studies based on the analysis of the distribution of young open clusters (Dias et al. 2002; Mermilliod & Paunzen 2003) and classical long-period Cepheids (Berdnikov et al. 2000) confirm the presence of a gap in the distribution of young objects along the Sagittarius–Carina arm (Majaess, Turner & Lane 2009). This fact needs very accurate interpretation, because spiral arms can have patchy structure. On the other hand, the different kinematics of these regions suggests that they could belong to different outer rings (Paper I).

Note that the inner ring in sketch B is larger and less elongated than that in sketch A (Fig. 8). Probably this larger ring corresponds to a case in which the inner rings form further away from the bar (Grouchy et al. 2010). Nevertheless, both types of inner ring can be associated with the 3-kpc arm and its counterpart (Fux 1999; Dame & Thaddeus 2008; Rodriguez-Fernandez & Combes 2008).

At the moment we cannot say which conditions determine the exact placing and shape of the inner ring-like structures and those of outer rings R_1 in sketches A and B. In principle, the difference between them may be related to the different kinds of orbits creating them: the very pointed inner ring in sketch A could be formed by the 'classical' orbits that are found in barred potentials (Contopoulos & Grosbol 1989), whereas the rings/pseudo-rings in sketch B could be formed by manifold orbits (Athanassoula et al. 2010).

Our sketches also exhibit conspicuous differences in the shape and orientation of nuclear gas condensation: in sketch A it is more round and elongated perpendicular to the bar while in sketch B it is oriented along the bar and looks like a secondary bar (Erwin 2011, and references therein). All our models have two ILRs located at distances $R_{ILR} = 0.2$ and 1.5 kpc (Papers I and II), so the difference between them cannot be caused by their position. Probably it appears due to some features of the gas inflow. Special

numerical simulations of the gas flow in the central region of the Galaxy show that a 1-kpc nuclear ring can be holed and contain additional elliptical gas condensation with semi-axes of $a \approx 200$ and $b \approx 100$ pc, which are associated with the Central Molecular Zone (CMZ: Ferriére 2008; Rodriguez-Fernandez & Combes 2008), but our models do not have enough resolution to reproduce this detail.

5.4 Kinematic distances

Most giant star-forming complexes have only kinematic distances, which were calculated from kinematic models with a purely circular rotation law. Russeil (2003) reckons that photometric distances for stars exciting H II regions are determined with errors of 20–30 per cent. The errors in kinematic distances depend on the direction but, on average, the deviations of velocity $V_{\rm LSR}$ from the rotation curve of 15 km s^{-1} correspond to an error of ∼20 per cent in kinematic distances. This estimation was derived under the assumption that we always made a correct choice between 'far' and 'near' distances on the same line of sight, but non-circular gas motions significantly complicate this choice. In the case of a wrong choice, the distance error can exceed 100 per cent.

We compared the observed $V_{\rm LSR}$ velocities of giant star-forming complexes from the catalogue by Russeil et al. (2007) with model velocities of gas particles in a model with an analytical bar (Paper I). For each complex, we selected model particles located within 200 pc of the observed position of a complex (l, r) and calculated their mean velocity along the line of sight. The mean difference between the model and observed $V_{\rm LSR}$ velocities is found to be $\Delta V = 16$ km s^{-1}, which does not exceed significantly the mean difference between the observed $V_{\rm LSR}$ velocity and velocity calculated from the model rotation curve $\Delta V = 11$ km s^{-1}. Formally, the kinematic distances by Russeil et al. (2007) are quite reasonable.

The scale of kinematic distances is determined by the distance scale of objects used for calculation of the rotation curve. If distances for the objects studied and the rotation curve are self-consistent, then velocity deviations from the rotation curve are always minimal and practically independent of the distance scale chosen.

Fig. 9 shows model $V_{\rm LSR}$ velocities calculated for different heliocentric distances r of the star-forming complex 372 ($l = 311.^\circ2$, $b = -0.^\circ4$) in the catalogue by Russeil et al. (2007). We selected model particles (gas and OB) located within 200 pc from the chosen position of the complex and calculated their model $V_{\rm LSR}$ velocity. The number of model particles N within a 200-pc circle is also shown. The positions of the rings correspond to the maxima on curve $N(r)$. For each r we also determine the $V_{\rm LSR}$ velocity through the model rotation curve. We can see that complex 372 can be moved from the distance $r = 11.3$ to 10.2 kpc to fall exactly on ring R_2, and its new position is in good agreement with the observed $V_{\rm LSR}$.

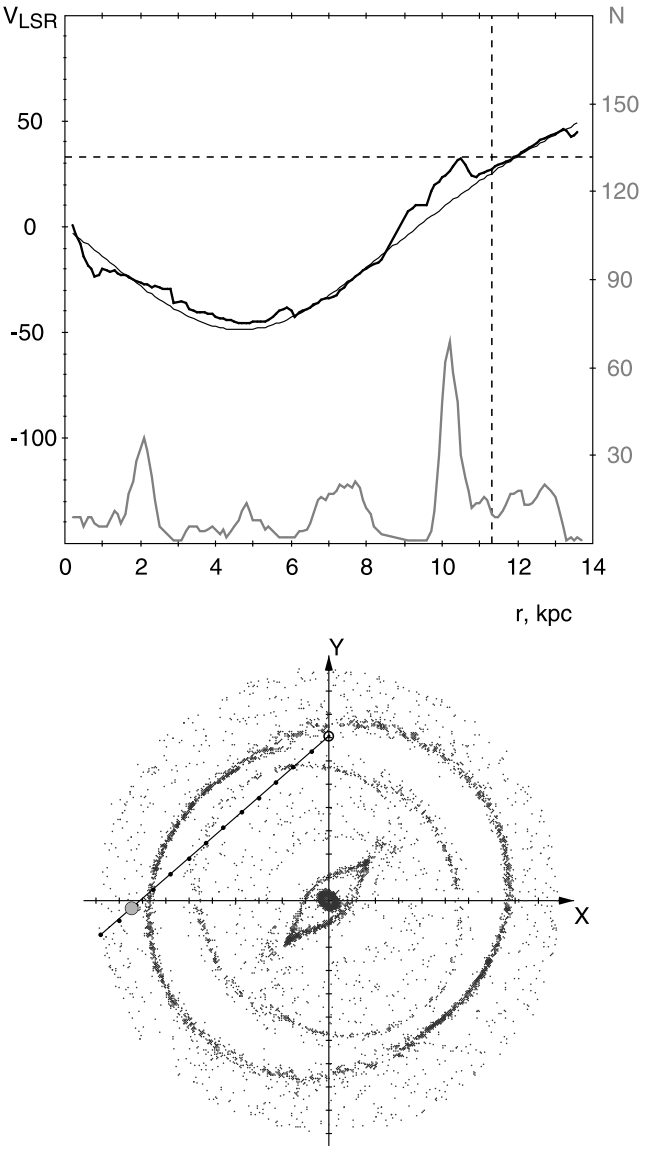

Figure 9. Upper: Model $V_{\rm LSR}$ velocities (black thick line) calculated for different heliocentric distances r of the star-forming complex 372 ($l = 311.^\circ2$, $b = -0.^\circ4$, Russeil et al. 2007). Dashed lines indicate the observed $V_{\rm LSR}$ velocity ($V_{\rm LSR} = 33.0$ km s^{-1}) and the catalogue value of the kinematic distance reduced to a short distance scale ($r = 11.3$ kpc). The grey line indicates the number of particles N within a 200-pc circle at the chosen r. The left vertical axis (black) shows the scale for $V_{\rm LSR}$ velocities while the right axis (grey) exhibits the scale for N. The thin black line indicates $V_{\rm LSR}$ calculated through the model rotation curve. Lower: position of complex 372 in the Galactic plane with respect to the distribution of model particles (Paper I). The line of sight with 1-kpc divisions is also shown.

6 CONCLUSIONS

A model of the Galaxy with an outer ring R_1R_2' can explain some large-scale morphological features of Galactic spiral structure. Ascending segments of the rings can be regarded as fragments of the trailing spiral arms, descending ones as fragments of the leading arms. We found that the Carina arm falls well on the ascending segment of ring R_2. Note also that the objects of the Sagittarius arm are located near the ascending segment of ring R_1. The Carina–Sagittarius arm can consist of two ascending segments of outer rings R_1 and R_2, which almost touch each other near the Carina region. It is possible that another pair of ascending segments of the outer rings can be identified with the Norma–Cygnus arm symmetrical to the Carina–Sagittarius one. The Perseus and Crux arms can be partially identified with the descending segments of ring R_2. Thus, the two-component outer ring R_1R_2' can be mistakenly interpreted as a four-armed spiral pattern.

Fourier analysis of a distribution of OB associations with the same kinematic characteristics over spiral harmonics shows the presence of a leading component in the spiral structure of the Galaxy (Mel'nik 2005). The sample includes OB associations with radial component of velocity V_R directed toward the Galactic Centre. The appearance of the leading spiral agrees with the position of the Sun near the

descending segment of ring R_2, which can be thought as a fragment of the leading spiral arm.

A model of a two-component outer ring could also explain the existence of some tangential directions corresponding to emission maxima near the terminal velocity curves. Model diagrams (l, $V_{\rm LSR}$) reproduce the maxima in the direction of the Carina, Crux, Norma and Sagittarius arms. Additionally, a N-body model yields maxima in the directions of the Scutum and 3-kpc arms.

On the basis of numerical simulations, we propose two sketches of the ring structure of the Galaxy that include a bar, two outer rings, an inner ring and nuclear gas condensation forming a nuclear ring and/or secondary bar (Fig. 8). Both sketches can explain the position of the Carina–Sagittarius arm with respect to the Sun. Sketch A can also explain the existence of an excess of old stars in the direction of the Centaurus arm, $l \approx -50^\circ$.

ACKNOWLEDGMENTS

We thank Heikki Salo for the use of his simulation code. We are grateful to N. Ya. Sotnikova and P. Grosbol for useful remarks and interesting discussion. This work was partly supported by the Russian Foundation for Basic Research (project nos. 10-02-00489).

REFERENCES

Adler D. S., Roberts W. W., 1992, ApJ, 384, 95
Anderson L. D., Bania T. M., 2009, ApJ, 690, 706
Athanassoula E., 1984, Phys. Rep., 114, 321
Athanassoula E., 1992, MNRAS, 259, 328
Athanassoula E., Romero-Gómez M., Bosma A., Masdemont J. J., 2010, MNRAS, 407, 1433
Babusiaux C., Gilmore G., 2005, MNRAS, 358, 1309
Benjamin R. A. et al., 2005, ApJ, 630, L149
Berdnikov L. N., Dambis A. K., Vozyakova O. V., 2000, A&AS, 143, 211
Bertin G., Lin C. C., 1996, Spiral Structure in Galaxies: A Density Wave Theory. MIT Press, Cambridge, MA
Binney J., Tremaine S., 2008, Galactic Dynamics, 2nd edn. Princeton Univ. Press, Princeton, NJ
Binney J., Gerhard O., Stark A. A., Bally J., Uchida K. I., 1991, MNRAS, 252, 210
Bissantz N., Gerhard O., 2002, MNRAS, 330, 591
Bissantz N., Englmaier P., Gerhard O., 2003, MNRAS, 340, 949
Blaha C., Humphreys R. M., 1989, AJ, 98, 1598
Blitz L., Spergel D. N., 1991, ApJ, 379, 631
Blitz L., Binney J., Lo K. J., Bally J., Ho P. T. P., 1993, Nat, 361, 417
Burton W. B., Bania T. M., 1974, A&A, 33, 425
Burton W. B., Shane W. W., 1970, in Becker W., Contopoulos G. I., eds, Proc. IAU Symp. 38, The Spiral Structure of our Galaxy. Reidel, Dordrecht, p. 397
Buta R., 1986, ApJS, 61, 609
Buta R., 1995, ApJS, 96, 39
Buta R., Combes F., 1996, Fund. Cosmic Phys., 17, 95
Buta R., Crocker D. A., 1991, AJ, 102, 1715
Buta R., Corwin H. G., Odewahn S. C., 2007, The de Vaucouleurs Atlas of Galaxies. Cambridge Univ. Press, Cambridge
Byrd G., Rautiainen P., Salo H., Buta R., Crocker D. A., 1994, AJ, 108, 476
Cabrera-Lavers A., Hammersley P. L., González-Fernández C., López-Corredoira M., Garzón F., Mahoney T. J., 2007, A&A, 465, 825
Caswell J. L., Haynes R. F., 1987, A&A, 171, 261
Chakrabarty D., 2007, A&A, 467, 145
Churchwell E. et al., 2009, PASP, 121, 213
Cohen R. S., Dame T. M., Thaddeus P., 1986, ApJS, 60, 695
Contopoulos G., Grosbol P., 1989, A&AR, 1, 261
Contopoulos G., Papayannopoulos Th., 1980, A&A, 92, 33
Dambis A. K., Mel'nik A. M., Rastorguev A. S., 1995, Astron. Lett., 21, 291
Dambis A. K., Mel'nik A. M., Rastorguev A. S., 2001, Astron. Lett., 27, 58
Dame T. M., Thaddeus P., 2008, ApJ, 683, L143
Dame T. M., Elmegreen B. G., Cohen R. S., Thaddeus P., 1986, ApJ, 305, 892
Dame T. M., Hartmann D., Thaddeus P., 2001, ApJ, 547, 792
Dehnen W., 2000, AJ, 119, 800
Dias W. S., Alessi B. S., Moitinho A., Lepine J. R. D., 2002, A&A, 389, 871
Downes D., Wilson T. L., Bieging J., Wink J., 1980, A&AS, 40, 379
Drimmel R., 2000, A&A, 358, L13
Efremov Yu. N., 1998, Astron. Astrophys. Trans., 15, 3
Efremov Yu. N., 2011, Astron. Rep., 55, 108
Englmaier P., Gerhard O., 1999, MNRAS, 304, 512
Englmaier P., Gerhard O., 2006, Celest. Mech. Dynam. Astron., 94, 369
Erwin P., 2011, Mem. Soc. Astron. Ital. Suppl., 18, 145
Ferriére K., 2008, Astron. Nachr., 329, 992
Fux R., 1999, A&A, 345, 787
Fux R., 2001, A&A, 373, 511
Georgelin Y. M., Georgelin Y. P., 1976, A&A, 49, 57
Gerhard O., 2011, Mem. Soc. Astron. Ital. Suppl., 18, 185
Glushkova E. V., Dambis A. K., Mel'nik A. M., Rastorguev A. S., 1998, A&A, 329, 514
Grabelsky D. A., Cohen R. S., Bronfman L., Thaddeus P., 1988, ApJ, 331, 181
Grouchy R. D., Buta R. J., Salo H., Laurikainen E., 2010, ApJ, 139, 2465
Habing H. J., Sevenster M. N., Messineo M., van de Ven G., Kuijken K., 2006, A&A, 458, 151
Henderson A. P., Jackson P. D., Kerr F. J., 1982, ApJ, 263, 116
Hou L. G., Han J. L., Shi W. B., 2009, A&A, 499, 473
Humphreys R. M., 1976, ApJ, 206, 114
Humphreys R. M., 1979, in Burton W. B., ed., Proc. IAU Symp. 84, The Large-Scale Characteristics of the Galaxy. Reidel, Dordrecht, p. 93
Humphreys R. M, McElroy D. B., 1984, ApJ, 284, 565
Kalberla P. M. W., Berton W. B., Hartmann D., Arnal E. M., Bajaja E., Morras R., Pöppel W. G. L., 2005, A&A, 440, 775
Kalnajs A. J., 1973, Proc. Astron. Soc. Australia, 2, 174
Kalnajs A. J., 1991, in Sundelius B., ed., Dynamics of Disc Galaxies. Göteborgs Univ., Göthenburg, p. 323
Kerr F. J., 1962, MNRAS, 123, 327
Kerr F. J., 1970, in Becker W., Contopoulos G. I., eds, Proc. IAU Symp. 38, The Spiral Structure of our Galaxy. Reidel, Dordrecht, p. 95
Levine E. S., Blitz L., Heiles C., 2006, Sci, 312, 1773
Lin C. C., Shu F. H., 1964, ApJ, 140, 646
Lin C. C., Yuan C., Shu F. H., 1969, ApJ, 155, 721
Lockman F. J., 1979, ApJ, 232, 761
Majaess D. J., Turner D. G., Lane D. J., 2009, MNRAS, 398, 263
Masset F., Tagger M., 1997, A&A, 322, 442
Mel'nik A. M., 2003, Astron. Lett., 29, 304
Mel'nik A. M., 2005, Astron. Lett., 31, 80
Mel'nik A. M., 2006, Astron. Lett., 32, 7
Mel'nik A. M., Dambis A. K., 2009, MNRAS, 400, 518
Mel'nik A. M., Rautiainen P., 2009, Astron. Lett., 35, 609 (Paper I)
Mel'nik A. M., Dambis A. K., Rastorguev A. S., 1999, Astron. Lett., 25, 518
Mel'nik A. M., Dambis A. K., Rastorguev A. S., 2001, Astron. Lett., 27, 521
Mermilliod J.-C., Paunzen E., 2003, A&A, 410, 511
Mihalas D., Binney J., 1981, Galactic Astronomy, 2nd edn. Freeman & Co., San Francisco
Minchev I., Boily C., Siebert A., Bienayme O., 2010, MNRAS, 407, 2122
Oort J. H., Kerr F. J., Westerhout G., 1958, MNRAS, 118, 379
Paladini R., Davies R. D., DeZotti G., 2004, MNRAS, 347, 237
Pohl M., Englmaier P., Bissantz N., 2008, ApJ, 677, 283
Rastorguev A. S., Pavlovskaya E. D., Durlevich O. V., Filippova A. A., 1994, Astron. Lett., 20, 591
Rautiainen P., Mel'nik A. M., 2010, A&A, 519, 70 (Paper II)

Rautiainen P., Salo H., 1999, A&A, 348, 737
Rautiainen P., Salo H., 2000, A&A, 362, 465
Roberts W. W., 1972, ApJ, 173, 259
Rodriguez-Fernandez N. J., Combes F., 2008, A&A, 489, 115
Russeil D., 2003, A&A, 397, 133
Russeil D., Adami C., Georgelin Y. M., 2007, A&A, 470, 161
Salo H., 1991, A&A, 243, 118
Salo H., Laurikainen E., 2000, MNRAS, 319, 377
Schwarz M. P., 1981, ApJ, 247, 77
Sellwood J. A., 2000, Ap&SS, 272, 31
Sellwood J. A., 2011, MNRAS, 410, 1637
Sellwood J. A., Kahn F. D., 1991, MNRAS, 250, 278
Sellwood J. A., Lin D. N. C., 1989, MNRAS, 240, 991
Sellwood J. A., Sparke L. S., 1988, MNRAS, 231, 25
Simonson S. C., 1970, A&A, 9, 163
Sitnik T. G., 2003, Astron. Lett., 29, 311
Sitnik T. G., Mel'nik A. M., 1996, Astron. Lett., 22, 422
Toomre A., 1977, ARA&A, 15, 437
Vallée J. P., 2005, AJ, 130, 569
Vallée J. P., 2008, AJ, 135, 1301
Watson C., Araya E., Sewilo M., Churchwell E., Hofner P., Kurtz S., 2003, AJ, 587, 714
Weiner B. J., Sellwood J. A., 1999, ApJ, 524, 112

This paper has been typeset from a TEX/LATEX file prepared by the author.